AIAA 81-0996R

Composite Three-Dimensional Grids Generated by Elliptic Systems

P. D. Thomas*
Lockheed Palo Alto Research Laboratory, Palo Alto, Calif.

A technique is presented for constructing a boundary-conforming grid throughout a general three-dimensional flow region as a composite of subregion grids. Each subregion grid is generated numerically by solving a nonlinear system of elliptic equations. The boundary values represent nodal points in a quasi-two-dimensional grid that covers the curved surface bounding the subregion, and are generated numerically by a modified elliptic system. A primary feature of the technique is that the composite three-dimensional grid remains both continuous and smooth across the surface of juncture between any two adjoining subregions. Sample results are given for a wing-body combination.

I. Background

A GENERAL method for constructing boundary-conforming grids within arbitrarily shaped two-dimensional plane flow regions has been given by Thompson et al.[1] The method may be viewed as a mapping of the physical flow region onto a rectangle in a transformed plane. The mapping transformation is represented as the solution to an elliptic boundary-value problem for the rectangle, governed by a system of Poisson equations. For a simply-connected flow region, Dirichlet boundary values are specified that represent the physical coordinates of grid points located on the boundaries of the physical flow region. For multiply-connected regions, branch cuts are introduced that permit the mapping onto a single rectangle. Boundary values (grid point locations) may not be assigned along the branch cuts, hence one has no direct control over the grid point distribution in the neighborhood of the cuts. However, the grid point distribution in the vicinity of the cuts or in other parts of the interior of the flow region can be controlled by the artful selection of source terms in the generating system of Poisson equations. This is true also of simply-connected regions.

The original method of Thompson et al.[1] has been modified by Thomas and Middlecoff[2,3] to provide automatic control over the grid point distribution in the interior of the flow region. In the modified method, the interior grid is controlled directly by the grid point distribution assigned on the boundaries (i.e., by the Dirichlet boundary values). This is accomplished by the use of source terms in the Poisson equations whose mathematical form is independent of the boundary shape and of the boundary grid point distribution. The source terms contain free parameters that are evaluated locally at the boundaries using limiting forms of the elliptic equations and are interpolated into the interior. Solved numerically, the elliptic system then generates an interior grid that reflects both the geometric shape of the boundary and the spatial distribution of grid points along the boundary.

The modified method allows one to control directly both the angle with which transverse grid lines intersect the boundary and the local curvature of the transverse grid lines at the boundary.[3] In particular, the transverse grid lines can be made locally orthogonal to the boundary. This makes it possible to treat multiply-connected regions by subdividing them into simply-connected subregions for which the Dirichlet problem remains well-posed. Continuity and smoothness of the grid lines across the artificial boundaries between subregions is a natural consequence of the method.[3] Even for simply-connected regions, this division into subregions may be used to enhance local control of the interior grid, and allows one to employ grids having different topological structures in different subregions while maintaining overall continuity and smoothness of the composite grid formed from the union of subregion grids.

The method of Thompson et al.[1] has been extended to three dimensions by Mastin and Thompson[4] and has been applied to several model aircraft and missile configurations by Thames.[5] In analogy with the two-dimensional case, a three-dimensional flow region is mapped onto a rectangular parallelepiped. The mapping transformation is computed numerically as the solution to an elliptic boundary value problem for the parallelepiped.

II. Overview

In the present paper, the method of Thomas and Middlecoff[3] is extended to three dimensions and is applied to a wing-body combination typical of aircraft configurations. For such applications, the general procedure is outlined in the following.

To begin, the three-dimensional flow region about the configuration is subdivided into a collection of contiguous simply-connected subregions. The surfaces that separate adjoining subregions may be selected for convenience, and need not be planar. A three-dimensional grid is then generated for each subregion. To simplify the description of how this is accomplished, we shall assume that the subregion is bounded by six differentiable surfaces, each of which separates the subregion from an adjacent subregion. Then the subregion so bounded may be mapped directly onto a unit cube. Under the mapping, each face of the cube is the image of one of the surfaces that bound the physical subregion itself.

The mapping transformation, and hence the grid throughout the physical subregion, is obtained numerically as the solution to a Dirichlet problem for the cube. This approach relies on the method of Thompson et al.[1] as generalized to three dimensions by Mastin and Thompson,[4] except that the source terms in the elliptic system are a generalization of those employed in two dimensions by Thomas and Middlecoff.[2,3] As in the two-dimensional case, the source terms involve free parameters that must be computed from Dirichlet boundary values specified at the six faces of the computational cube. For each such face, these boundary values represent the coordinates of nodal points in a

Presented as Paper 81-0996 at the AIAA 5th Computational Fluid Dynamics Conference, Palo Alto, Calif., June 22-23, 1981; submitted June 23, 1981; revision received Dec. 7, 1981.

*Staff Scientist, Applied Mechanics Laboratory. Member AIAA.

quasi-two-dimensional grid covering that surface segment of the physical subregion which maps onto the face in question. Thus, to obtain the boundary values for the three-dimensional problem, we must first construct a set of six two-dimensional grids, one for each surface segment that bounds the physical subregion. If the surface segment is planar, then the method of Thomas and Middlecoff[3] is used to generate the two-dimensional grid. For a curved surface such as a fuselage or wing, an extension of the latter method allows one to generate a quasi-two-dimensional grid that lies upon the curved surface. Once the boundary values have been obtained in this fashion for all faces of the computational cube, the three-dimensional grid is generated by a technique similar to that employed in the two-dimensional case.

In what follows, we first review in Sec. III the general technique for two dimensions to lay the foundation for later extension to higher dimensions. Then, in Sec. IV, we show how the method can be generalized to permit construction of quasi-two-dimensional grids on curved surfaces. The extension to three dimensions is developed in Sec. V. Finally, Sec. VI illustrates the application of the technique to generate a composite three-dimensional grid suitable for computing the flowfield about a simple wing-body combination.

III. Plane Two-Dimensional Grids

Given a simply-connected region of the (x,y) plane such as that illustrated in Fig. 1, the technique presented by Thomas and Middlecoff[2,3] generates a boundary-conforming coordinate transformation

$$x,y \rightarrow \xi,\eta$$

that maps the region onto a rectangle (Fig. 2). The transformation is generated numerically as the solution to an elliptic boundary-value problem governed by the following system of equations.†

$$\nabla^2\xi = \phi(\xi,\eta)\,|\,\nabla\xi\,|^2 \qquad \nabla^2\eta = \psi(\xi,\eta)\,|\,\nabla\eta\,|^2 \qquad (1)$$

where ϕ,ψ are free parameters that are to be computed from Dirichlet boundary values (x,y) specified along the boundary OABCO in the physical plane (Fig. 1).

These equations are transformed to ξ,η coordinates by interchanging the roles of dependent and independent variables. This yields an elliptic system of quasilinear equations that can be written in the vector form

$$\alpha(r_{\xi\xi}+\phi r_\xi) - 2\beta r_{\xi\eta} + \gamma(r_{\eta\eta}+\psi r_\eta) = 0 \qquad (2)$$

$$r = (x,y) \qquad (3a)$$

$$\alpha = |\,r_\eta\,|^2, \qquad \beta = r_\xi \cdot r_\eta, \qquad \gamma = |\,r_\xi\,|^2 \qquad (3b)$$

The nonlinear coefficients in Eq. (3b) are scalars that represent the metric coefficients of the transformation. The system Eq. (2) is solved numerically on a uniform rectangular grid

$$\xi_j = (j-1)\Delta\xi, \qquad 1 \le j \le J$$

$$\eta_k = (k-1)\Delta\eta, \qquad 1 \le k \le K$$

where we have chosen

$$\Delta\xi = 1/(J-1) \qquad \Delta\eta = 1/(K-1)$$

so that the computational region is a unit square in the ξ,η plane.

†It recently has been brought to the author's attention that source terms of the form employed on the right-hand side of Eqs. (1) and in Refs. 2 and 3 had been used earlier by Shanks and Thompson.[6]

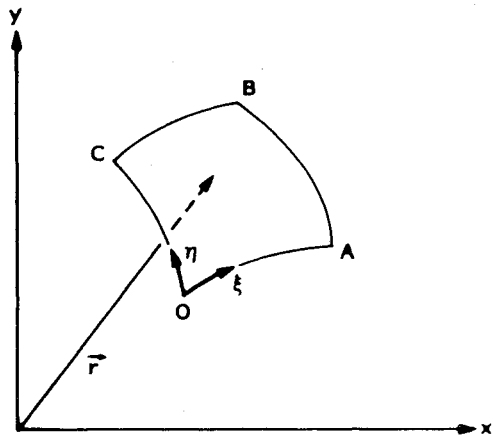

Fig. 1 Two-dimensional physical region.

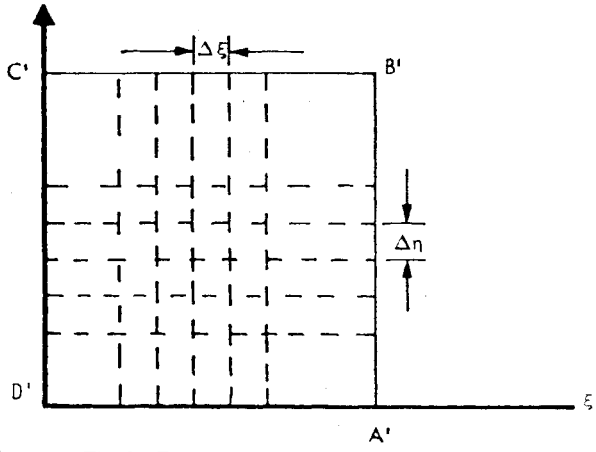

Fig. 2 Rectangular computational domain.

Boundary values r_{jk} are assigned along the perimeter of O′A′B′C′O′ of the square. These boundary values represent the coordinates (x,y) of grid points along the perimeter OABCO of the physical region, and may be distributed in any fashion desired. Appropriate limiting forms of Eq. (2) are used to evaluate the parameters ϕ,ψ locally along the boundary of the square, where r is known from the assigned boundary values. The parameters then are interpolated into the interior to obtain a continuous representation $\phi(\xi,\eta)$, $\psi(\xi,\eta)$ throughout the square, and the elliptic system Eq. (2) is solved numerically by some suitable method such as SLOR iteration.

The parameters ϕ,ψ are evaluated individually along each of the four segments of the boundary in the ξ,η plane. For later reference, we shall review in detail how the evaluation is accomplished. Consider, for example, the lower horizontal segment O′A′, which represents a coordinate curve $\eta = \text{const}$ along which ξ alone varies. The vector r_ξ is locally tangent to the corresponding boundary segment OA in the physical plane, whereas the vector r_η is locally tangent to the coordinate curves $\xi = \text{const}$ that are transverse to the boundary segment.

In general, to evaluate ϕ or ψ uniquely along the boundary segment, constraints must be imposed on the local slope and curvature with which the transverse $\xi = \text{const}$ curves meet the boundary segment.[3] For example, one may constrain the transverse coordinate curves to be orthogonal to the boundary segment

$$r_\xi \cdot r_\eta = 0 \qquad \text{on O′A′B′C′O′} \qquad (4)$$

Under this constraint, one may obtain a single scalar equation for the parameter ϕ by taking the projection of Eq. (2) onto the boundary segment; that is, by taking the scalar product of r_ξ with Eq. (2). The resulting equation can be cast in the form

$$\phi = -(T_0 + |r_\xi| T_1) \tag{5a}$$

$$T_0 = (r_\xi \cdot r_{\xi\xi})/|r_\xi|^2 \tag{5b}$$

$$T_1 = (r_\xi \cdot r_{\eta\eta})/(|r_\xi| |r_\eta|^2) \tag{5c}$$

The ξ-differentiated quantities T_0 and $|r_\xi|$ in Eqs. (5) can be evaluated numerically from the assigned boundary values using standard difference operators to represent the differential operators. However, the term T_1 involves η derivatives which cannot be evaluated locally from boundary data alone.

One can show that, under the orthogonality constraint Eq. (4), the term T_0 is simply the logarithmic derivative of arc length with respect to the parameter ξ along the boundary segment[3]; whereas T_1 is the local curvature of the transverse grid lines $\xi = \text{const}$. Thus, if we impose the additional constraint that the curvature of the transverse grid lines must vanish at the boundary, $T_1 = 0$, then the parameter ϕ can be computed directly in terms of the distribution of arc length between grid points assigned along the boundary segment OA (Ref. 3). Although this procedure works well in many cases, as shown by the examples presented in Ref. 3, it fails to yield an adequate interior grid in situations where the transverse boundary segment AB or CO has substantial intrinsic curvature. As an extreme example, one can show analytically that Eq. (2) cannot generate even a simple equispaced polar coordinate system when the parameter ϕ is evaluated from Eq. (5) with the zero-curvature constraint $T_1 = 0$ imposed. Although one could specify any desired curvature distribution $T_1(\xi)$ along the boundary segment OA as a constraint, it is more expedient to use the curvature of the transverse boundaries AB,CO to control the curvature of the transverse grid lines in the interior. The curvature T_1 can be computed at the endpoints of the segment OA by using one-sided difference formulas to approximate the ξ and η derivatives in Eq. (5c). Simple linear interpolation of the radius of curvature $1/T_1$ vs arc length $s = \int |r_\xi| \, d\xi$ then yields a representation of $T_1(\xi)$ over the rest of the boundary segment OA for use in evaluating the parameter ϕ from Eq. (5a). The same procedure is employed to evaluate the parameter $\phi(\xi)$ along the upper boundary segment BC in Fig. 2. A continuous representation $\phi(\xi,\eta)$ throughout the interior of the square is then obtained by linear interpolation as a function of η along vertical mesh lines $\xi = \text{const}$.

$$\phi_{j,k} = \phi_{j,1} + (\phi_{j,K} - \phi_{j,1})(k-1)/(K-1) \tag{6}$$

The same technique can be applied to evaluate the parameter $\psi(\eta)$ along the vertical boundary segments AB,CO from the equation obtained by taking the scalar product of Eq. (2) with the vector r_η, and to compute $\psi(\xi,\eta)$ by interpolation along horizontal mesh lines $\eta = \text{const}$. Once having defined the parameters ϕ,ψ throughout the computational square in Fig. 2, the elliptic system is solved to obtain the grid point coordinates $r = (x,y)$ in the physical domain of Fig. 1.

The described approach has two primary attributes. First, control over the interior grid is achieved by using only the geometric shape of the boundary and the assigned distribution of grid points along the boundary segments. Since the spacing of grid points between the endpoints of each boundary segment can be parametrized easily in terms of a single quantity, the arc length, the user need not be burdened with the task of manipulating individual grid points, but may distribute grid points along each boundary segment with the aid of a general one-dimensional stretching function such as that devised by Vinokur.[7] Second, as stated in Sec. I, a continuous and smooth composite grid that covers a given region can be constructed by subdividing the region into smaller subregions for which individual grids are generated independently. The composite grid remains continuous and smooth across each boundary segment that separates contiguous subregions as long as the same boundary values are used at that common boundary segment when generating the grid for either subregion flanking the boundary.[3] This is a natural consequence of using the boundary values to evaluate the parameters ϕ,ψ that enter into the generating elliptic system Eq. (2).

IV. Quasi-Two-Dimensional Grids on Curved Surfaces

The described technique can be extended to generate grids on curved as well as plane surfaces. Let the surface be defined in Cartesian coordinates by the function $z = f(x,y)$, where f is single valued and twice differentiable. Then a set of equations for the projection of the grid onto the x-y plane is (see Appendix)

$$|r_\eta|^2 (x_{\xi\xi} + \phi x_\xi) - 2(r_\xi \cdot r_\eta) x_{\xi\eta} + |r_\xi|^2 (x_{\eta\eta} + \psi x_\eta) + f_x G = 0 \tag{7a}$$

$$|r_\eta|^2 (y_{\xi\xi} + \phi y_\xi) - 2(r_\xi \cdot r_\eta) y_{\xi\eta} + |r_\xi|^2 (y_{\eta\eta} + \psi y_\eta) + f_y G = 0 \tag{7b}$$

$$r = (x,y,z), \qquad z = f(x,y) \tag{7c}$$

$$G = J_2^2 [(1+f_y^2) f_{xx} - 2 f_x f_y f_{xy} + (1+f_x^2) f_{yy}] / (1+f_x^2+f_y^2) \tag{7d}$$

$$J_2 = \partial(x,y)/\partial(\xi,\eta) = x_\xi y_\eta - x_\eta y_\xi \tag{7e}$$

where J_2 denotes the two-dimensional Jacobian determinant. Equations (7a,b) become identical to the system Eq. (2) in the plane case $f = 0$, but take account of both the slope and curvature of the surface $f(x,y)$. In exactly the same fashion that the latter system is used to generate a plane grid, Eqs. (7) can be used to generate a grid within any closed, simply-connected region that lies on the surface $z = f(x,y)$. Equation (5) remains valid for evaluating the parameter ϕ along boundary segments $\eta = \text{const}$ provided that the radius vector r is interpreted in the three-dimensional sense of Eq. (7c) rather than in the two-dimensional sense of Eq. (3a). The corresponding equation for the parameter ψ at boundary segments $\xi = \text{const}$ may be obtained from Eq. (5) by introducing the substitution $(\phi,\xi,\eta) \rightarrow (\psi,\eta,\xi)$.

V. Three-Dimensional Grids

Mastin and Thompson[4] have devised an elliptic system that can be used to map a three-dimensional bounded region onto the unit cube in a transformed computational space ξ, η, ζ. Upon introducing the three-dimensional counterpart of the source terms employed in the two-dimensional system of Eqs. (1), the corresponding three-dimensional elliptic system can be written as

$$\alpha_1 (r_{\xi\xi} + \phi r_\xi) + \alpha_2 (r_{\eta\eta} + \psi r_\eta) + \alpha_3 (r_{\zeta\zeta} + \omega r_\zeta) + 2(\beta_1 r_{\xi\eta} + \beta_2 r_{\eta\zeta} + \beta_3 r_{\zeta\xi}) = 0 \tag{8}$$

$$r = (x,y,z) \tag{9}$$

$$\alpha_1 = J_3^2 (\nabla\xi \cdot \nabla\xi) \quad \alpha_2 = J_3^2 (\nabla\eta \cdot \nabla\eta) \quad \alpha_3 = J_3^2 (\nabla\zeta \cdot \nabla\zeta)$$
$$\beta_1 = J_3^2 (\nabla\xi \cdot \nabla\eta) \quad \beta_2 = J_3^2 (\nabla\eta \cdot \nabla\zeta) \quad \beta_3 = J_3^2 (\nabla\zeta \cdot \nabla\xi) \tag{10}$$

The gradients of the transformed coordinates in Eqs. (10) are given by[8]

$$\nabla\xi = J_3^{-1}(r_\eta \times r_\zeta)$$

$$\nabla\eta = J_3^{-1}(r_\zeta \times r_\xi)$$

$$\nabla\zeta = J_3^{-1}(r_\xi \times r_\eta) \tag{11}$$

where J_3 denotes the Jacobian determinant of the inverse transformation

$$J_3 = \frac{\partial(x,y,z)}{\partial(\xi,\eta,\zeta)} \tag{12}$$

For later use, we observe that the quantities α_i,β_i that appear in Eq. (8) can be written in terms of the metric coefficients of the transformation simply by inserting Eqs. (11) into the definitions Eqs. (10) and expanding the repeated vector and scalar products to obtain

$$\alpha_1 = (|r_\eta|\,|r_\zeta|)^2 - (r_\eta \cdot r_\zeta)^2$$

$$\alpha_2 = (|r_\zeta|\,|r_\xi|)^2 - (r_\zeta \cdot r_\xi)^2$$

$$\alpha_3 = (|r_\xi|\,|r_\eta|)^2 - (r_\xi \cdot r_\eta)^2$$

$$\beta_1 = (r_\eta \cdot r_\zeta)(r_\zeta \cdot r_\xi) - (r_\xi \cdot r_\eta)|r_\zeta|^2$$

$$\beta_2 = (r_\zeta \cdot r_\xi)(r_\xi \cdot r_\eta) - (r_\eta \cdot r_\zeta)|r_\xi|^2$$

$$\beta_3 = (r_\xi \cdot r_\eta)(r_\eta \cdot r_\zeta) - (r_\zeta \cdot r_\xi)|r_\eta|^2 \tag{13}$$

In analogy with the two-dimensional case discussed in Sec. III, the parameters ϕ,ψ,ω are computed locally from boundary values assigned at the faces of the computational cube, and are then interpolated into the interior of the cube. Under the mapping, each face is the image of one of the surface segments that bound the physical region, and the boundary values represent the coordinates of nodal points in a quasi-two-dimensional grid that covers the surface segment (see Figs. 3 and 4). Consider, for example, the upper and lower surfaces $\zeta=0,1$. As in the two-dimensional case, the parameters can be evaluated locally in terms of boundary values, provided that constraints are imposed on the slope and curvature of the family of ζ-directed grid lines transverse to the boundary surface segment. The simplest case results if this family is taken orthogonal to the boundary. For the boundaries $\zeta=$ const, this orthogonality constraint may be stated as

$$r_\zeta \cdot r_\xi = 0, \qquad r_\zeta \cdot r_\eta = 0, \quad \text{on } \zeta = 0,1 \tag{14}$$

which follow from the fact that the vectors r_ξ, r_η are locally tangent to the boundary surface, whereas the vector r_ζ is locally tangent to the transverse coordinate lines. The coefficients β_2,β_3 then vanish, and α_2,α_3 are correspondingly simplified.

A further simplification results if the boundary values come from a ξ,η surface grid which itself is orthogonal, for then we have

$$r_\xi \cdot r_\eta = 0 \tag{15}$$

Two independent uncoupled equations for evaluating the parameters ϕ,ψ at either boundary $\zeta=0,1$ then can be obtained by taking the scalar product of Eq. (8) with the vectors r_ξ, r_η, respectively, which lie in the tangent plane. The resulting equation for ϕ is

$$\phi = -[T_0 + |r_\xi| T_1' + T_2] \text{ on } \zeta = 0,1 \tag{16a}$$

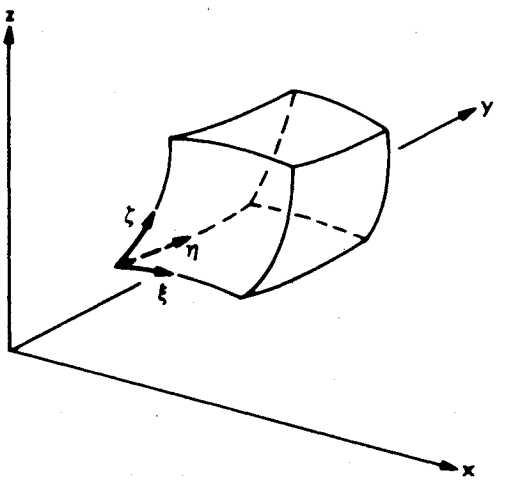

Fig. 3 Three-dimensional physical region.

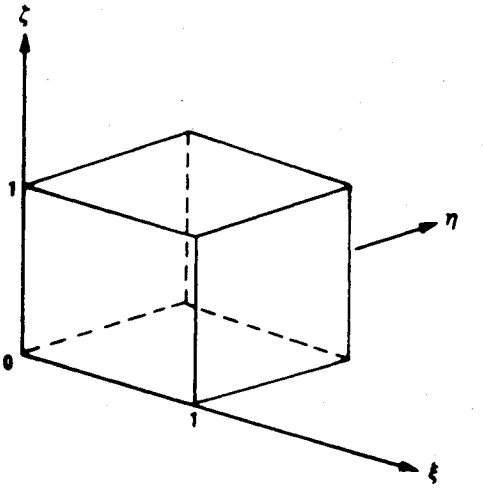

Fig. 4 Cubical computational domain.

where T_0 is given by Eq. (5b) using Eq. (9), and

$$T_1' = (r_\xi \cdot r_{\xi\zeta})/(|r_\xi|\,|r_\zeta|^2), \quad T_2 = (r_\xi \cdot r_{\eta\eta})/|r_\eta|^2 \tag{16b}$$

As in the two-dimensional case, T_0 and $|r_\xi|$ can be evaluated directly from the boundary values that are assigned at $\zeta=0$ or $\zeta=1$. The term T_2 also can be evaluated directly. The quantity T_1' can be interpreted physically in terms of the local curvature of ζ-directed transverse grid lines, and can be evaluated in the same fashion as the corresponding quantity T_1 in Eq. (5c) for the two-dimensional case. That is, we use the known curvature of the ζ-directed grid lines in the transverse boundary surfaces $\xi=0,1$.

In the more general case where the ξ,η grid on a boundary surface $\zeta=0,1$ is not orthogonal, Eqs. (15) and (16) no longer hold, but the same approach can be employed to evaluate the parameters ϕ,ψ. Upon taking the scalar product of Eq. (8) with r_ξ and with r_η, one obtains a pair of linear equations that can be solved easily to obtain unique expressions for evaluating ϕ and ψ in terms of the given boundary values at $\zeta=0,1$. The described procedure is used to evaluate all three parameters ϕ,ψ,ω at the faces of the computational cube. In general, this defines each parameter at four of the six faces. One can infer from the structure of Eq. (8) that the parameter ϕ is associated primarily with the spacing of grid points along ξ-directed coordinate lines. This inference is consistent with the fact that the described procedure for evaluating ϕ from boundary values at the faces of the cube defines ϕ at only those four faces in which ξ is an interior coordinate

parameter. This excludes the two faces $\xi = \text{const}$. Similarly, ψ is defined at all save the two faces $\eta = \text{const}$, and ω at all save the faces $\zeta = \text{const}$.

In analogy with the two-dimensional case, our aim is to project the parameters ϕ, ψ, ω smoothly into the interior of the cube from the faces at which they have been evaluated using boundary values. The elliptic system Eq. (8) then merely constitutes an elaborate mechanism for interpolating the surface grids into the interior of the physical region. The following very simple method of projecting the parameters into the interior of the cube appears to be adequate. Consider, for example, the parameter ϕ which is known at the four faces $\zeta = 0,1$ and $\eta = 0,1$. In each plane ξ-const, $0 \le \xi \le 1$, of the computational cube, we have a square $0 \le \eta, \zeta \le 1$ on whose perimeter ϕ is known. A simple way of projecting ϕ smoothly into the interior of the square to obtain a continuous representation $\phi(\xi, \eta, \zeta)$ is to use the general solution to the equation $\phi_{\eta\eta\zeta\zeta} = 0$ which can be integrated analytically. This is an elementary extension of the one-dimensional linear interpolation method that we have used successfully for two-dimensional grids,[3] in the sense that it reduces to the latter when one drops to two dimensions from three.

The described three-dimensional formulation can be used in concert with the surface grid generation technique presented in Sec. IV to construct a three-dimensional grid within an arbitrary spatial region such as that depicted in Fig. 3. One proceeds as follows. First, the technique of Sec. IV is used to generate a quasi-two-dimensional grid over each surface segment that bounds the region. This requires the a priori selection of a very small subset of nodal points in the three-dimensional grid, namely, those points which lie along the curves of intersection between the surface segments which bound the physical region. The bounding surfaces, and hence their curves of intersection, are known. The locations of grid points along each such curve can be parametrized easily in terms of the arc length, and the points may be distributed along the curve with the aid of a general one-dimensional coordinate-stretching function.[7]

Once the surface grids have been constructed, the surface grid point coordinates are used as the boundary values for the three-dimensional Dirichlet problem on the cube. The free parameters that enter into the source terms for the elliptic system are evaluated at the faces of the computational cube and are projected into the interior. The Dirichlet problem then is solved numerically by some iterative method.

This direct approach is likely to be inadequate for geometrically complicated regions, and is invalid for multiply-connected regions. These situations always can be treated by subdividing the region into a collection of contiguous simply-connected subregions, each of which has a more or less uniform geometric character. Each subregion grid is generated independently and is then joined with the others to form a composite grid for the original region. Although this subregion approach may appear cumbersome at first glance, note that any two contiguous subregions have a common boundary surface. The quasi-two-dimensional grid on that surface defines the Dirichlet boundary values for both subregions flanking the surface. This means that generally fewer than six individual quasi-two-dimensional surface grids need be generated per subregion.

An important feature inherent in the present method is that the composite grid automatically remains both continuous and smooth across the surface of juncture between any two adjacent subregions as long as the same boundary values are used at that common surface when generating the grid for either subregion. This feature is a direct consequence of using the boundary values to evaluate the parameters ϕ, ψ, ω that enter into the generating elliptic system. An example of such a composite grid is presented in the next section.

VI. Application to a Simple Wing-Body Combination

The technique outlined in the preceding section has been applied to construct a three-dimensional grid about the simple wing-body combination depicted in Fig. 5. The configuration consists of a cylindrical fuselage with spherical end caps and a straight wing that has a superelliptical planform. The axis of the cylinder coincides with the Cartesian y axis, the wing midchord line coincides with the x axis, and the wing cross section is symmetric about the plane $z = 0$. In the positive half-space $z \ge 0$, the wing surface is generated by the equation

$$(\epsilon x)^n + y^n = [(\tau - z)(\tau^{-1} + z)]^{n/2}$$

$$\epsilon = 0.2, \qquad \tau = 0.25, \qquad n = 8$$

where τ is the thickness-to-chord ratio in the plane $x = 0$ and ϵ the chord-to-span ratio. The configuration is symmetric about each of the three coordinate planes $x = 0$, $y = 0$, and $z = 0$.

The surface grids shown in Fig. 5 on the cylinder, the sphere, and the wing were generated by the method described in Sec. IV, treating each of the three parts as an independent subregion.

To form a bounded region in which to construct a three-dimensional grid, the configuration is enclosed by an outer "freestream" boundary surface consisting of an elliptical cylinder with an end cap formed by the matching ellipsoid of revolution. Since the region is symmetric about the three coordinate planes, we consider only the positive octant $x, y, z \ge 0$, and include the planes $x = 0$ and $z = 0$ as boundaries. This region was subdivided into two subregions separated by the plane normal to the y axis that passes through the sphere-cylinder juncture of the body. A three-dimensional view of each of these subregions is given in Figs. 6 and 7, and shows the grid on each visible surface. Figure 8 shows the composite grid formed by joining the two subregions.

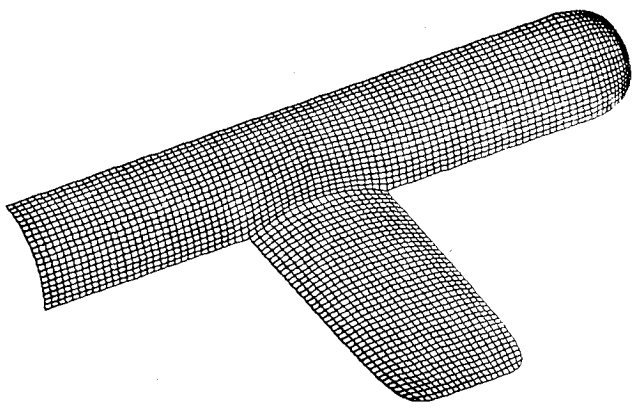

Fig. 5 View of wing-body combination showing surface grids.

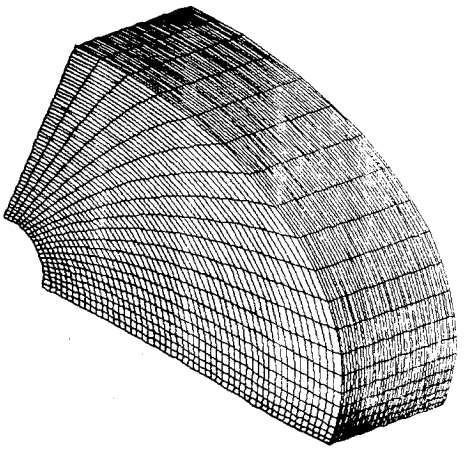

Fig. 6 View of aft subregion grid.

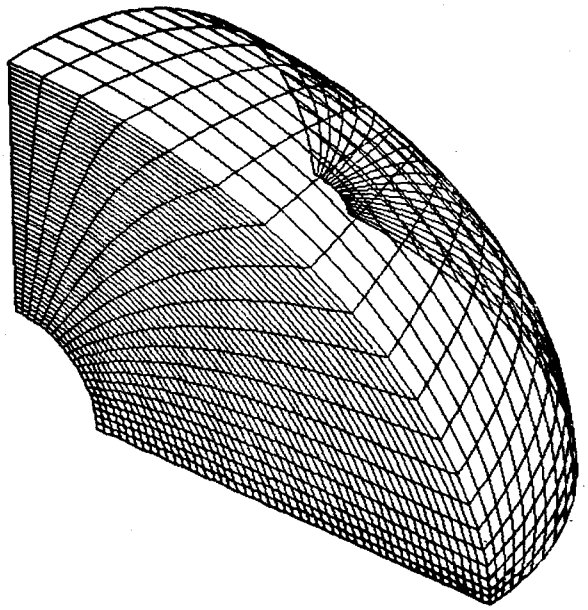

Fig. 7 View of forward subregion grid.

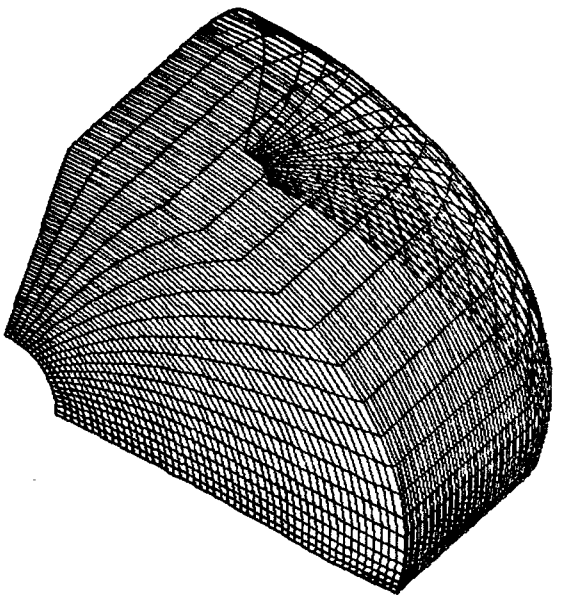

Fig. 8 View of composite grid.

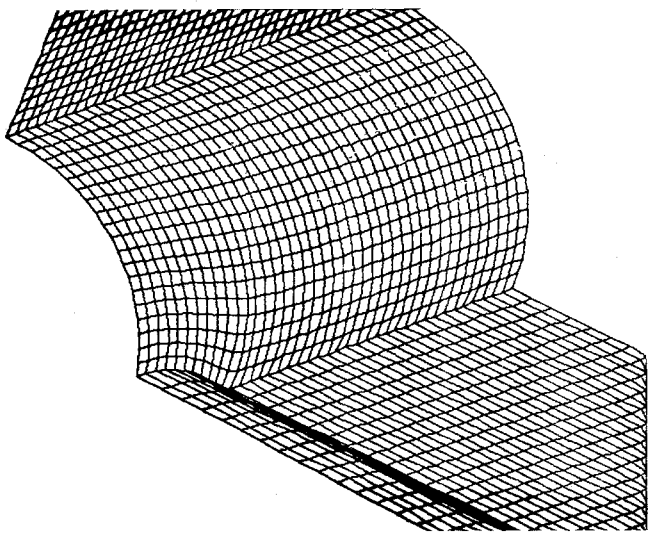

Fig. 9 Expanded view of grid on aft part of body, wing, and symmetry planes.

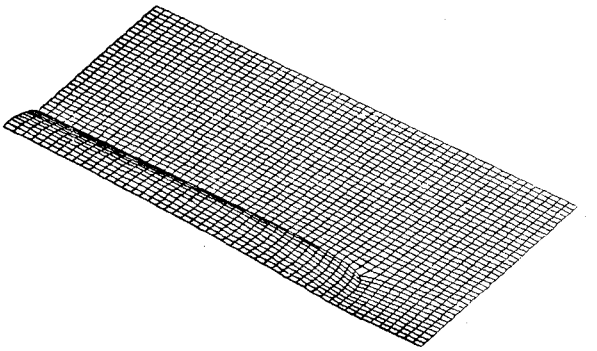

Fig. 10 Isolated view of composite surface grid on wing and horizontal symmetry plane.

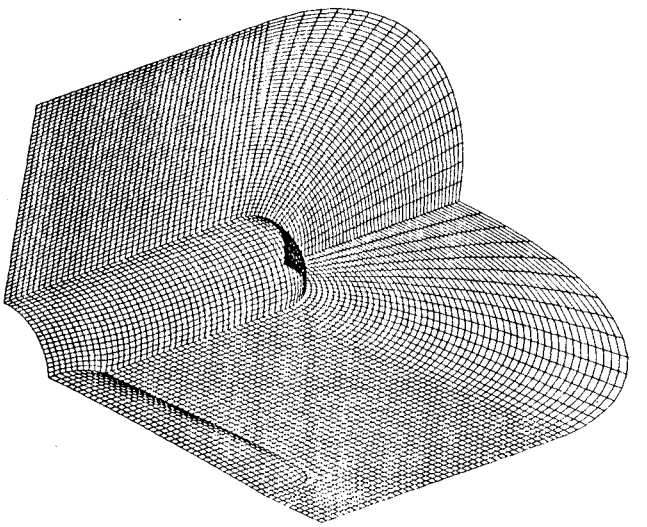

Fig. 11 Composite grid on wing, body, and symmetry planes.

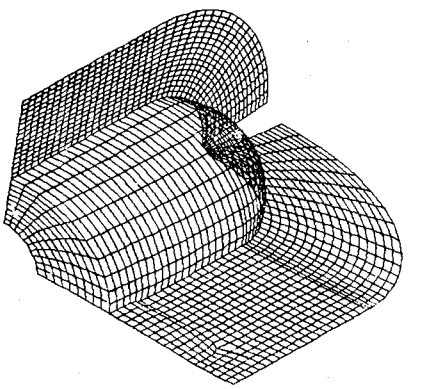

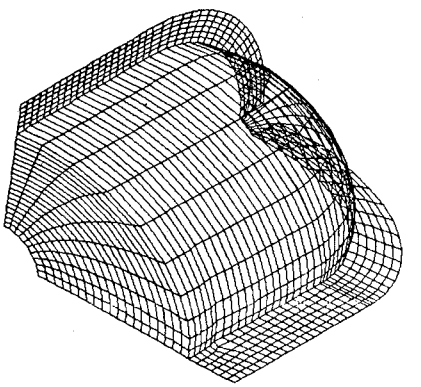

Fig. 12 Three-dimensional view of composite grid showing grid lines on an interior "body-like" coordinate surface.

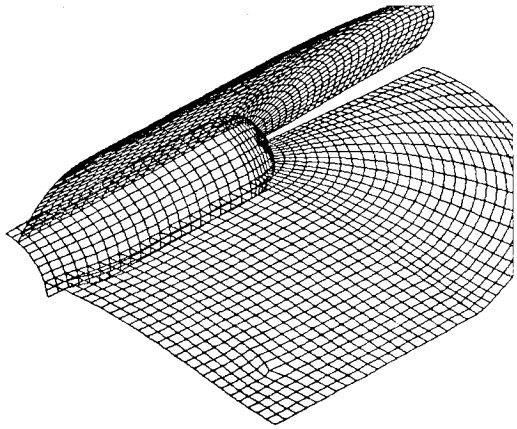

Fig. 13 Three-dimensional view of composite grid showing grid lines on body surface and on two interior "body-normal" coordinate surfaces.

An expanded view of the body surface grid near the wing root is given in Fig. 9. The latter also shows a portion of the vertical symmetry plane and the horizontal symmetry plane that form two of the boundaries for the aft subregion depicted in Fig. 6.

A separate view of the grids on the wing-surface and on the horizontal symmetry plane beyond the wing is displayed in Fig. 10. The two surface grids were generated separately by treating the wing surface and the symmetry plane as separate subregions with a common boundary curve, but the two form a single composite grid for the lower surface of the aft subregion of Fig. 6.

In Fig. 11, the surface grids on the nosecap and on the vertical and horizontal symmetry planes for the forward subregion of Fig. 7 have been joined to those displayed in Fig. 9 to show that grid lines remain smooth between adjoining subregions. This smoothness also is evident in Figs. 12 and 13, which display several interior coordinate surfaces of the composite grid.

The number of grid points in each of the two subregions depicted in Figs. 6 and 7 is $26\times11\times21\approx6000$. For each subregion, solution of the elliptic system by successive line over-relaxation (SLOR) required approximately 150 iterations and 15 min of CPU time on a VAX 11/780 minicomputer.

Appendix: Derivation of Elliptic System for Quasi-Two-Dimensional Grids on Curved Surfaces

Here we present a derivation of Eq. (7) of Sec. IV, which can be used to generate a grid on a curved surface

$$z=f(x,y) \tag{A1}$$

The basic idea is to start with the three-dimensional elliptic system Eq. (8), to deduce from it a limiting form which involves only quantities that are defined locally within a coordinate surface, and then to identify that surface with the given surface Eq. (A1). To accomplish this, let the latter surface be represented as a coordinate surface $\zeta=$ const in the ξ,η,ζ parameter space to which Eq. (8) applies. Because ξ,η coordinate curves lie within the surface, we are at liberty to impose constraints on the behavior of the ζ-directed transverse coordinate lines in order to simplify Eq. (8) as much as possible. To this end, we take the transverse coordinate lines to be orthogonal to the surface $\zeta=$ const and require that their principal curvature vanish locally.

Orthogonality is expressed by Eqs. (14). The principal curvature C of a space curve such as a ζ-directed coordinate line is defined classically so that the rate of turning of the local tangent vector

$$t=r_\zeta/|r_\zeta| \tag{A2}$$

with respect to arc length

$$ds=|r_\zeta|\,d\zeta \tag{A3}$$

is given by[9]

$$\frac{dt}{ds}=Cp \tag{A4}$$

where the unit vector p is orthogonal to t. Upon inserting Eqs. (A2) and (A3) into Eq. (A4) and performing the indicated differentiation, the result can be cast in the form

$$r_{\zeta\zeta}=|r_\zeta|^2Cp+(|r_\zeta|_\zeta/|r_\zeta|)r_\zeta \tag{A5}$$

For $C=0$, this reduces to

$$r_{\zeta\zeta}=(|r_\zeta|_\zeta/|r_\zeta|)r_\zeta \tag{A6}$$

This last equation along with the orthogonality constraints Eqs. (14) simplify the vector Eq. (8) to a form in which the third scalar component can be used to eliminate the quantity ω from the first two component equations. The resulting two scalar equations are

$$\begin{aligned}&|r_\eta|^2[x_{\xi\xi}+\phi x_\xi+u(z_{\xi\xi}+\phi z_\xi)]-2(r_\xi\cdot r_\eta)(x_{\xi\eta}+uz_{\xi\eta})\\&\quad+|r_\xi|^2[x_{\eta\eta}+\psi x_\eta+u(z_{\eta\eta}+\psi z_\eta)]=0\\&|r_\eta|^2[y_{\xi\xi}+\phi y_\xi+v(z_{\xi\xi}+\phi z_\xi)]-2(r_\xi\cdot r_\eta)(y_{\xi\eta}+vz_{\xi\eta})\\&\quad+|r_\xi|^2[y_{\eta\eta}+\psi y_\eta+v(z_{\eta\eta}+\psi z_\eta)]=0\end{aligned} \tag{A7}$$

where

$$u=-x_\zeta/z_\zeta \qquad v=-y_\zeta/z_\zeta \tag{A8}$$

The direction ratios u,v may be evaluated in terms of quantities that involve only ξ and η derivatives by using the orthogonality conditions Eqs. (14) as follows. Upon expanding the scalar products in Eqs. (14) and introducing the definitions Eqs. (A8), one obtains a pair of equations that are linear in u and v and that can be solved to obtain

$$u=J_2^{-1}(z_\xi y_\eta-z_\eta y_\xi) \qquad v=J_2^{-1}(z_\xi x_\eta-z_\eta x_\xi) \tag{A9}$$

where J_2 is given by Eq. (7e) of Sec. IV.

Equations (A7) and (A9) together represent a limiting form of the elliptic system Eq. (8) that involves only interior derivatives with respect to the parameters ξ,η within the surface $\zeta=$ const. We now introduce the equation of the surface, Eq. (A1), and expand the ξ and η derivatives of f by the chain rule

$$z_\xi=f_xx_\xi+f_yy_\xi \qquad z_\eta=f_xx_\eta+f_yy_\eta \tag{A10}$$

It follows from Eqs. (A9) and (A10) that the direction ratios are simply

$$u=f_x, \qquad v=f_y \tag{A11}$$

Substitution of Eqs. (A10) and (A11) into Eqs. (A7) then yields a pair of equations that can be manipulated algebraically in a straightforward fashion to obtain the system given in Eqs. (7) of Sec. IV.

Acknowledgment

The author is indebted to Mrs. K. L. Neier, who programmed the equations, carried out their solution, and created the three-dimensional plots to display the results. This work was sponsored by the NASA Ames Research Center.

References

[1]Thompson, J. F., Thames, F. C., and Mastin, C. S., "Boundary-Fitted Curvilinear Coordinate Systems for Solution of Partial Differential Equations on Fields Containing any Number of Arbitrary Two Dimensional Bodies," *Journal of Computational Physics,* Vol. 15, 1974, pp. 299-319.

[2]Middlecoff, J. F. and Thomas, P. D., "Direct Control of the Grid Point Distribution in Meshes Generated by Elliptic Equations," AIAA Paper 79-1462, July 1979.

[3]Thomas, P. D. and Middlecoff, J. F., "Direct Control of the Grid Point Distribution in Meshes Generated by Elliptic Equations," *AIAA Journal,* Vol. 18, July 1980, pp. 652-656.

[4]Mastin, C. W. and Thompson, J. F., "Transformation of Three Dimensional Regions onto Rectangular Regions by Elliptic Systems," *Numerical Mathematics,* Vol. 29, No. 4, 1978, pp. 397-407.

[5]Thames, F. C., "Numerical Generation of Three Dimensional Body-Fitted Curvilinear Coordinate Systems for Fluid Dynamics Calculations," Open Forum Paper, AIAA 3rd Computational Fluid Dynamics Conference, Albuquerque, N. Mex., 1977.

[6]Shanks, S. P. and Thompson, J. F., "Numerical Solution of the Navier-Stokes Equations for 2D Hydrofoils in or Below a Free Surface," *Proceedings of the Second International Conference on Numerical Ship Hydrodynamics,* Univ. of Calif. Extension Publs., Sept. 1977.

[7]Vinokur, M., "On One-Dimensional Stretching Functions for Finite-Difference Calculations," NASA CR 3133, Oct. 1980.

[8]Thomas, P. D. and Lombard, C. K., "The Geometric Conservation Law and Its Application to Flow Computations on Moving Grids," *AIAA Journal,* Vol. 17, Oct. 1979, pp. 1030-1037.

[9]Franklin, P., *Methods of Advanced Calculus,* McGraw-Hill, New York, 1944, pp. 107-109.